Impact of 'redox' cycles on performances of solid oxide fuel cells: Case of the electrolyte supported cells

J. Laurencin*, G. Delette, O. Sicardy, S. Rosini, F. Lefebvre-Joud

CEA/LITEN/DTH/LEV, 17 rue des martyrs 38054 Grenoble, France

ABSTRACT

Nickel with yttria stabilised zirconia (Ni-YSZ) is usually used as anode material for the solid oxide fuel cells (SOFCs) technology. Upon cyclic reduction and oxidation of Ni-YSZ ceramic–metal (cermet), the induced cell degradation constitutes one of the main limitations to the SOFCs lifetime. In this study, the effect of anode reduction and oxidation cycling on typical electrolyte supported cell (ESC) has been investigated. The electrochemical degradation has been followed by impedance spectroscopy. The cell damage has been characterised after testing with scanning electron microscopy (SEM). It has been shown that cells can withstand several 'redox' cycles without major decrease in electrochemical performances. The 'redox' cycling induces only a slight degradation rate estimated to $\sim$70 mΩ cm^2 per cycle. The microstructural observations are found to be consistent with the impedance diagram analysis. Both reveal that the damage is restricted to bulk cermet microstructure change, whereas no cracking is initiated at the anode/electrolyte interface.

© 2009 Elsevier B.V. All rights reserved.

1. Introduction

Solid oxide fuel cells (SOFCs) ensure the conversion of chemical energy into electricity at high temperatures. This kind of fuel cells represents a promising technology as they allow reaching high electrical efficiencies compared to conventional combustion system [1,2]. However, for practical applications, the robustness of SOFC systems is strongly impacted by some operating conditions. Basically, the accumulation of start and shutdown can lead to severe degradation of the SOFCs performance. When hydrogen supply is interrupted at high temperature, air may enter into the anode compartment. Unfortunately, the Ni-YSZ cermet, usually employed as SOFC anode material, is strongly sensitive to oxidising atmosphere. Indeed, at the operating temperature (typically 800 °C), the Ni-YSZ oxidation process is significantly faster in comparison to Ni powder [3,4]. Thus, the Ni phase in the cermet can be rapidly transformed into its oxidised state after the system shutdown. Therefore, repeated starts and stops due to the system management can be accompanied by cermet reduction and re-oxidation cycling. During these 'redox' cycles, the composite has to accommodate high dimensional change of Ni particles. Indeed, the oxidation of Ni into NiO involves a strong reversible expansion of the metallic particles due to the difference between the densities of each form ($\Delta V/V$ $\sim$40%).

The cermet is manufactured in its oxidised state and then reduced at the beginning of operation. The transformation of NiO into Ni leads to a strong shrinkage of the nickel phase. Therefore, this first reduction step is accompanied by a strong increase of the cermet porosity. It has been reported by several authors [4–6] that this step occurs without significant macroscopic deformation of the cermet. When re-oxidation happens, since nickel phase has undergone a prior coarsening upon operation, the NiO particles do not reoccupy their initial volume within the YSZ structure. As a consequence, the volume expansion due to the Ni transformation generates stresses and micro-cracks in the YSZ frame, resulting in an irreversible anodic macroscopic bulk expansion [4–7]. The linear strain of the cermet, ranging within 0–1%, depends mainly on the degree of oxidation [8] or on microstructure parameters such as porosity or Ni content [4]. Two mechanisms have been proposed to explain the nickel particles coarsening which is involved in this kind of cermet degradation. Malzbender et al. [9] and Sarantaridis et al. [6] have observed that re-oxidised NiO particles present higher inner porosity than initial ones. According to Klemenso et al. [5,10], the metal particle coarsening would be due to nickel redistribution and agglomeration, occurring under reducing atmosphere upon operation. However, as mentioned by Sarantaridis et al. [6], it is likely that both mechanisms are involved in the Ni coarsening.

In the case of the anode supported cell (ASC) design, the effect of 'redox' cycles has been widely studied [11–14]. Many authors have reported important electrochemical degradation after only one or few reduction and oxidation cycles. Indeed, it has been shown that the cermet bulk strain induced by the oxidation leads to high tensile

---

stresses in the thin electrolyte layer [15]. A conversion degree of Ni into NiO of about 50% is then sufficient to cause catastrophic failures of the dense and thin electrolyte [16,17].

Few studies have been devoted to the impact of the 'redox' cycles on the electrolyte supported cell (ESC) design. Cell stress state after the anode re-oxidation has been estimated through mechanical modelling approaches [15,18,19]. As the cermet cannot expand and remains constrained by the dense and thick electrolyte substrate, high compressive stresses are calculated within the thin NiO–YSZ layer. Under this specific loading, a delamination or a bulk degradation of the cermet layer is expected. Fouquet et al. [3] have carried out 'redox' cycling on classical ESC at 950 °C. An increase in the cell polarisation resistance of 18% has been obtained after the third 'redox' cycle. The authors have attributed the electrochemical degradation to cracks formed into the bulk cermet. Müller et al. [20] have studied the electrochemical degradation of ESC with a Ni-YSZ cermet consisting of small sized individual areas (pattern electrode) deposited on the thick electrolyte. 'Redox' cycles have also induced an increase in the cell polarisation resistance. The *post-mortem* observations have revealed a partial delamination of the anode and an agglomeration of Ni particles. Both microstructure evolutions are expected to reduce the cell electrochemical performances.

The present work is focused on the measurement and the analysis of the ESC degradation caused by the 'redox' cycling. For this purpose, three similar commercial cells have been oxidised under an air stream and then reduced under hydrogen. This 'redox' cycle has been repeated and the degradation of the cell has been followed by impedance spectroscopy. The diagrams evolution has been analysed and linked to the microstructural observations. A mechanical analysis of the test is proposed to explain the experimental results.

2. Experimental

2.1. Sample description

Experiments have been conducted using three specimens of the same commercial electrolyte supported cells manufactured by KERAFOL®. Fig. 1 shows a typical cross-section of cell observed by scanning electron microscopy (SEM). The dense electrolyte is 150 μm thick and presents a circular shape with a diameter of 55 mm. It is made up with 3 mol% yttria stabilised zirconia (3YSZ) (ZrO_2 stabilised with 3 mol% Y_2O_3). This 3YSZ material is chosen as support because of its high mechanical strength allowing the enhancement of the cell robustness. The cathode is a layer of ~50 μm in thickness, made with porous lanthanum doped strontium manganite (LSM) and deposited on one side of the electrolyte disk. The anode is layered on the other side of the electrolyte and
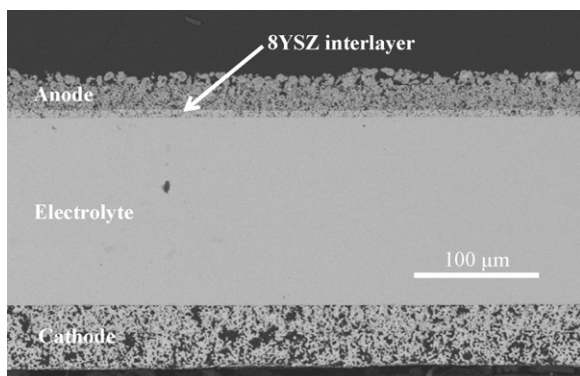

Fig. 1. Polished cross-section of the tested ESC examined by SEM (back scattered electron (BSE) image).
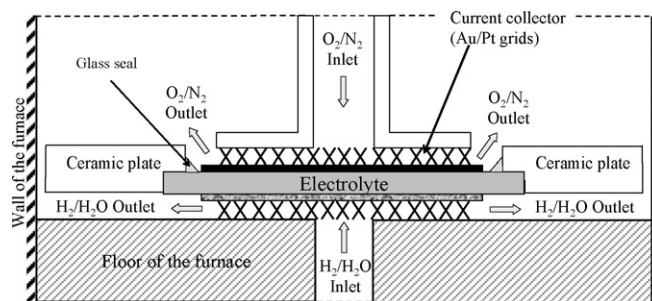

Fig. 2. Schematic representation of the electrochemical test bench. The pipes used to supply anode and cathode are made in alumina and present an internal diameter equal to 6 mm. The distance between the electrodes and the alumina plates for both anodic and cathodic channels is adjusted to 1 mm.

is composed of a porous composite of Ni and 8YSZ (ZrO_2 stabilised with 8 mol% Y_2O_3). This cermet presents a thickness of ~25 μm and a porosity of 31% in its oxidised state (NiO–8YSZ). A porous 8YSZ interlayer of ~7 μm in thickness is sandwiched between the dense electrolyte and the anode. The porosity of this interlayer is estimated to be ~15%. Both electrodes have a diameter of 40 mm and are centred on the electrolyte. The cell active area is around 12.5 cm^2.

2.2. Test procedures

Test bench configuration: The cells have been tested in the electrochemical test bench depicted in Fig. 2. Air and fuel channels present a radial co-flow arrangement where fluids are introduced at the cell centre and are exhausted from its periphery. At the anode side, the current collection is ensured by a gold grid with a mesh of 100 squares cm^{-2}. This grid is overlaid at the cathode side by a fine platinum mesh (3600 squares cm^{-2}). In order to minimize the contact resistances, a load of 480 g cm^{-2} is applied on the grids when the cell is in operation. The cell is sealed on its periphery with a flat ceramic ring, which avoids mixing air and fuel directly at the edge of the cell, and hence, prevents the post-combustion in this area. As the plate is manufactured in the same material than the electrolyte, no external loading is applied to the cell during the heating (or cooling) of the furnace.

Oxidation and reduction ('*redox*' *cycle*) *procedure*: Experiments have been carried out with a furnace temperature of 800 °C. After the initial reduction step of the NiO phase, the cermet has been re-oxidised under air stream. This 'redox' cycle has been repeated during the test according to the following sequences (the reference area used to normalize the flow rates corresponds to the cell active area equal to 12.5 cm^2):

(i) *Operation under reducing conditions*: Wet hydrogen ($H_2 + 3H_2O$) is sent to the anode side at a flow rate of $N_{H_2} = 16$ ml min^{-1} cm^{-2}.
(ii) The hydrogen flow is stopped and the fuel channels are swept under argon during 15 min ($N_{Ar} = 32$ ml min^{-1} cm^{-2}).
(iii) *Operation under oxidising conditions*: Gas supply at the anode side is switched to air flow during 30 min ($N_{Air} = 80$ ml min^{-1} cm^{-2}).
(iv) Air flow is stopped and the fuel channels are swept under argon during 15 min ($N_{Ar} = 32$ ml min^{-1} cm^{-2}).

All over the test, the air flow to the cathode side was maintained at 100 ml min^{-1} cm^{-2}. The cell electrochemical response has been followed by electrochemical impedance spectroscopy. Diagrams have been recorded under hydrogen, between each oxidising step, at open circuit voltage (OCV). A two electrodes configuration has been used. Diagrams have been measured with a Solartron
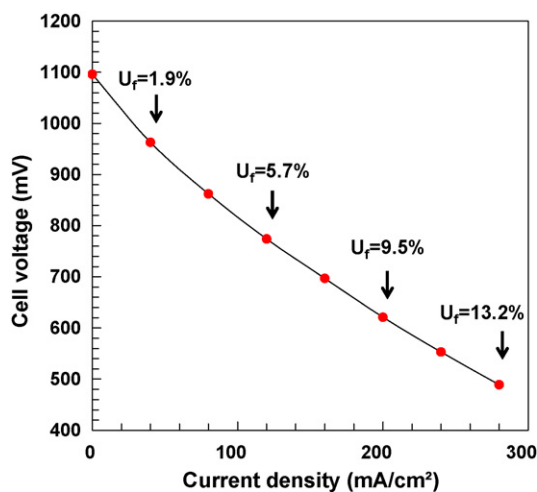
Fig. 3. Polarisation curve obtained under wet hydrogen (3% $H_2O + H_2$) for the second tested cell. Numbers added on the curve are related to the fuel utilisation Uf ($T_{furnace} = 800\,^{\circ}C$, $N_{H_2} = 16\,ml\,min^{-1}\,cm^{-2}$ and $N_{Air} = 80\,ml\,min^{-1}\,cm^{-2}$).

impedance analyser in the frequency range of (10 kHz to 0.1 Hz) and an applied current of $\Delta i = 120\,mA$.

Microstructural characterisations: The cell microstructure before and after operation has been analysed using a Zeiss Leo 1530 Scanning Electron Microscope equipped with a field emission gun (FEG). Cell cross-sections have been polished with diamond paste before observations and the samples were metallised by gold sputtering.

X-ray diffraction measurements: The degree of oxidation after the oxidising treatments has been measured by X-ray diffraction at room temperature. For this purpose, a cell sample has been previously heated up at 800 °C, reduced under hydrogen, and then re-oxidised in the same conditions than the ones carried out in the electrochemical experiments (*i.e. T* = 800 °C under an air stream during 30 min). To avoid any further change of the nickel oxidation state, air supply was replaced after the oxidising step by argon sweeping, and the sample was cooled down to the room temperature under this neutral atmosphere. This sample treatment was repeated twice in order to investigate the effect of the 'redox' cycles on diffractograms.

X-ray diffraction patterns were collected at room temperature on a two circles diffractometer, using Cu $K\alpha_{1,2}$ radiation and a position sensitive detector. Samples were mounted in an aluminium holder and scanned between $2\theta = 42.8°$ and $2\theta = 44.8°$ with $0.009°$ step size, counting 154 s per step.

3. Results and data analysis

3.1. Initial cell performances

Fuel cells performances are estimated through *i–V* curves, or polarisation curves, which give the evolution of the electrical current density generated as a function of the cell voltage. Fig. 3 shows a typical *i–V* curve obtained in this study under wet hydrogen (3% H_2O) at 800 °C (for the second tested cell). The cell voltage decreases when the current is rising as a result of irreversible losses related to (i) the charge transfer linked to the electrochemical reactions, (ii) the gas consumption and mass transport in the porous electrodes, (iii) the ionic resistance of the electrolyte and (iv) the current collection. It can be noticed that for the 3YSZ electrolyte supported cell, the contribution of the electrolyte (iii) is significant, but this kind of cells presents a very high mechanical stability.

Basically, the cell performances are improved by minimizing the irreversible losses. These effects, known as overpotentials,
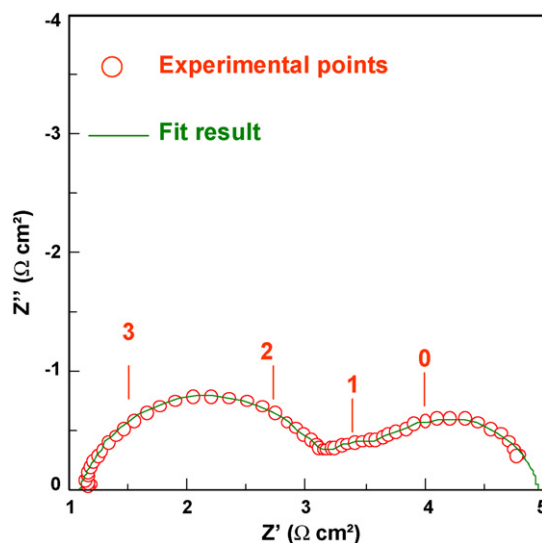

Fig. 4. Typical impedance diagram obtained under wet hydrogen at 800 °C (diagrams recorded after the 'redox' cycle no. 12 for the second tested cell). The diagram has been plotted in the complex plane. The numbers mark the decimal logarithm of the frequency. The solid line corresponds to the fit result obtained with the equivalent circuit given in Fig. 5.

depend on many parameters such as cell design, composition and microstructure.

Similar polarisation curves have been recorded for the three tested cells. It can be noticed that the electrochemical performances expected for this kind of cell are close to those obtained: the current density reaches $160\,mA\,cm^{-2}$ for a cell voltage of 0.7 V and a fuel utilisation of 7.57%.

3.2. Impedance diagrams of the tested cells

A typical impedance diagram obtained under reducing conditions ($3\%H_2O + H_2$) is plotted in Fig. 4 according to the Nyquist representation. The imaginary part Z'' of the cell impedance is plotted as a function of the real part Z' for all investigated frequencies. At the highest frequencies, the diagram is constituted by a purely resistive contribution, noted R_{ohmic}, which is classically attributed to the sum of two resistances: the current collecting resistance and the ionic resistance of the electrolyte (assuming that the electronic resistances of electrodes can be neglected). This resistive cell response at high frequencies is followed on the diagram by several semicircles at high, medium and low frequencies. These semicircles are representative of the electrochemical processes occurring at the electrodes.

As the cathode and anode electrochemical responses are entangled into the same frequency range [21], separating rigorously their respective contributions into the cell impedance diagrams are questionable. For this reason, in this work, a phenomenological approach has been adopted to fit the diagrams with an equivalent electrical circuit. As shown in Fig. 5, three semicircles at low, medium and high frequencies have been identified and represented
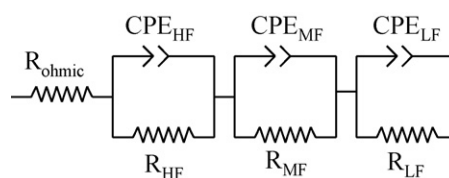

Fig. 5. Representation of the equivalent electrical circuit used to fit the impedance diagrams.
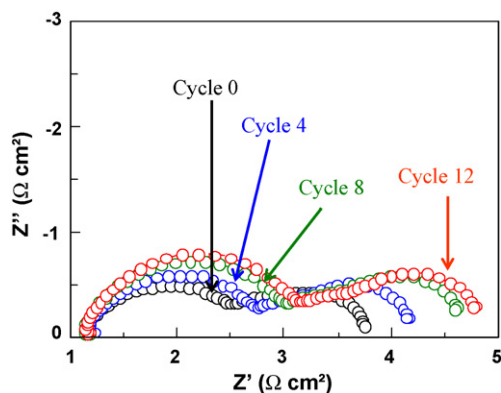
Fig. 6. Typical evolution of impedance diagrams according to the 'redox' cycle ($T_{furnace}$ = 800 °C, second tested cell). The diagram has been plotted in the complex plane.

Fig. 7. Cell resistances plotted as a function of the cycle number for the three tested cell. The filled markers correspond to the polarisation resistance and the open ones are related to the ohmic resistance.

by a resistance (R_{HF}, R_{MF} or R_{LF}) in parallel with a constant phase element (CPE_{HF}, CPE_{MF} or CPE_{LF}). The main purpose of this fit is the determination of the high frequency intercept (i.e. R_{ohmic}) and the polarisation resistance $R_{polarisation}$ induced by the electrodes overpotentials (i.e. $R_{polarisation} = R_{HF} + R_{MF} + R_{LF}$). During the 'redox' cycles, since only the atmosphere at the anode compartments is switched, it is expected that the diagram evolution is merely due to the anode degradation.

In order to determine the frequency range corresponding to the anode response, a sensitivity analysis of the impedance diagrams with hydrogen partial pressures at the anode compartments has been carried out. This study has been performed just after the initial evaluation of the cell performances by decreasing the hydrogen partial pressures from 0.73 to 0.24 atm. It has been found that the pure ohmic resistance R_{ohmic} is not affected by these atmosphere modifications. On the contrary, the sizes of the semicircles at low and high frequencies were strongly increased with decreasing the hydrogen partial pressure, indicating that the electrochemical response of the anode is mainly included in these two semicircles. Therefore, upon 'redox' cycles, it can be reasonably assumed that any evolution of these semicircles is linked to a degradation of the cermet electrochemical behaviour.

3.3. Impedance diagrams evolution during the 'redox' cycles

As illustrated in Fig. 6, after several 'redox' cycles, a global degradation of cell performances is noticed. This degradation has been quantified using the fit performed on impedance data obtained at each cycle. Fig. 7 provides the result of this impedance diagrams treatment: the high frequency intercept, R_{ohmic}, and the polarisation resistance, $R_{polarisation}$, have been plotted as a function the cycle number. A good reproducibility is observed between the three tested cells.

It is worth underlining that the ohmic resistances are not impacted by the 'redox' cycles. This result suggests that no delamination has occurred during the anode re-oxidation. Indeed, as calculated by Gazzari and Kesler [22–24] and observed by Laurencin et al. [17], cracks generation at the electrodes/electrolyte interface induces a decrease in effective cell active area, leading to a rise of the high frequency intercept on the impedance diagrams.

Inversely, the polarisation resistances of the three tested cells are found to increase with the 'redox' cycle numbers (Fig. 7). This degradation suggests that the anode re-oxidation steps have induced a bulk deterioration of the Ni-YSZ cermet, that has a direct impact on the electrochemical reactions, either the charge transfer or species transport.
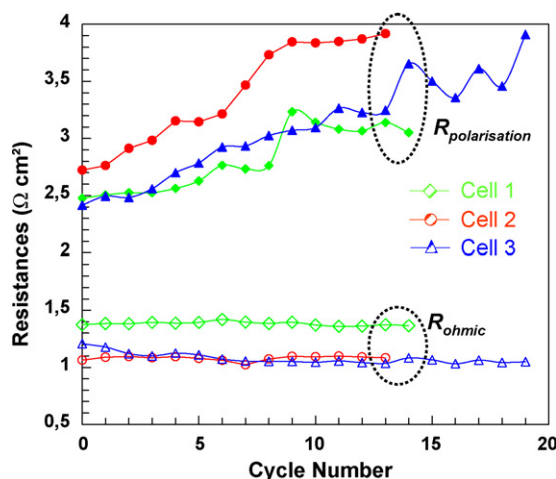
3.4. Microstructural characterisation

The microstructure of the cermet in its NiO–YSZ oxidised state has been examined by SEM before and after 'redox' cycles (Fig. 8). The observations are found to be consistent with the conclusions established with the electrochemical measurements.

Firstly, it was observed that electrolyte is undamaged. Moreover, since no crack was found at the cell interfaces (images b in Fig. 8), it is confirmed that no delamination has been initiated during the anode re-oxidations cycling. Inversely, as illustrated in Fig. 8, the cermet microstructure has been strongly impacted by the re-oxidation cycles. A bulk densification of the cermet is observed, than can explain the increase in the cell polarisation resistance.

3.5. X-ray diffraction

Whatever the number of the 'redox' cycle, the X-ray diffraction measurements have confirmed that the cermet is fully oxidised by the treatment under an air stream at 800 °C during 30 min. Furthermore, as illustrated in Fig. 9, it has been observed that the width of the NiO peak is strongly increased right from the first re-oxidation step (whereas the area of the peak remains unchanged). This trend could be explained either by a decrease of the nickel oxide grain sizes or by micro-strains in the NiO lattice.

4. Discussion

In the case of ASC design, it has been shown [17] that a degree of oxidation higher than 50% leads to catastrophic failure of the electrolyte, which allows the direct combustion of hydrogen with oxygen and prevents the fuel cell operation. Therefore, the strength of ASC design regarding the anode re-oxidation behaviour appears to be much lower than the ESC configuration. In agreement with previous studies performed on the ESC design [3,20], it has been shown in this work that such cell can withstand several full anode re-oxidation cycles without any damage of the electrolyte. In fact, the degradation rate of the polarisation resistance is found to be roughly equal to around 70 mΩ cm² per cycle, leading to an increase up to $\Delta R_{pol}/R_{pol,0} \sim 17\%$ after the sixth cycle. As the fuel cell continues to operate, electrolyte has not been cracked, and hence, the electrochemical degradation could be essentially attributed to an interfacial or bulk cermet damaging.
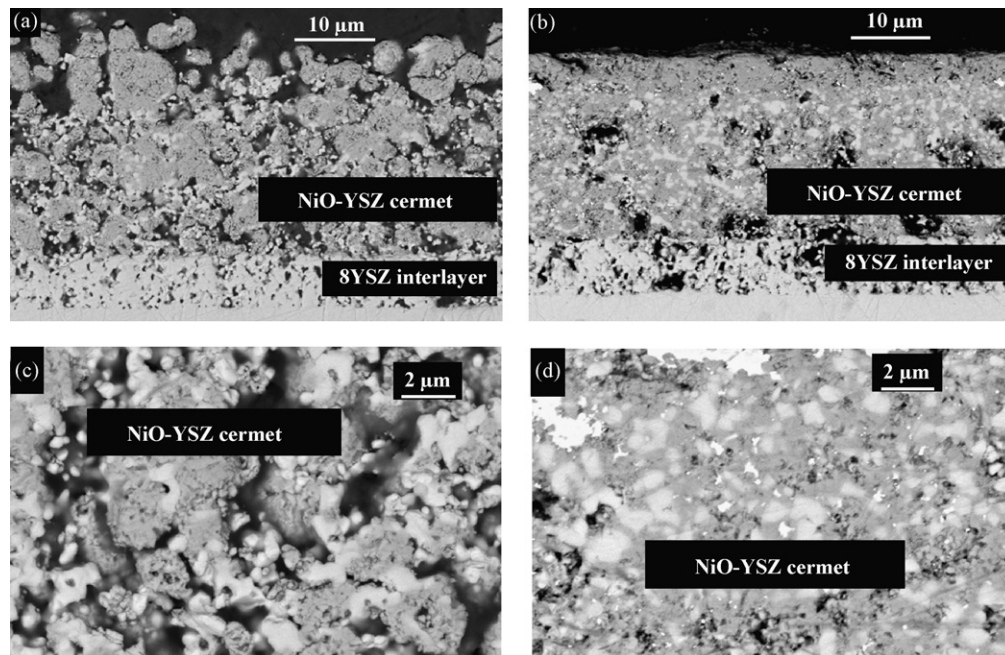
Fig. 8. Typical BSE–SEM images of the polished cell cross-section: (a and c) cells as received, and (b and d) no. 3 cell examined after the test (19th 'redox' cycle).

4.1. Delamination risk during the 'redox' cycling

A previous analysis of thermo-mechanical stresses during redox cycling [15] had pointed out that anode delamination had to be considered as a possible mode of ESC degradation. The experimental results presented in this study clearly show that no crack is initiated at the anode/electrolyte interface upon re-oxidation. The delamination risk in ESC can now be discussed considering both experimental and modelling approaches.

Basically, in the ESC configuration, the electrolyte substrate constrains the thin layer of cermet and prevents the expansion of the anode upon oxidation. Compressive stress develops and leads to an accumulation of elastic energy in the anode. If the amount of stored energy G exceeds the interfacial toughness G_c, the propagation of a crack between anode and electrolyte becomes possible. Both terms G and G_c of this criterion have to be evaluated separately.

The energy release rate G can be estimated through a simple mechanical analysis that takes into account (i) the loading, i.e. the strain of the anode induced by re-oxidation, and (ii) the materials properties [15]. It has to be mentioned that only data measured on thick specimens of cermet are available. Furthermore, this approach considers an undamaged and elastic behaviour of the anodic material. In the ESC configuration, these assumptions lead to values of G around 140 J m^{-2} for an anode fully oxidised ($\varepsilon_{ox} \sim 1\%$). However, this level has to be considered as an upper bound of the available energy. Indeed, two phenomena tend to decrease the actual level of loading in the cermet layer:

(i) The evolution of the microstructure observed after re-oxidation tends to indicate that a relaxation of mechanical stresses has occurred. It can be suggested that compressive stresses in the cermet have been the driving force that induces the microstructure densification illustrated by Fig. 8. This behaviour is specific to thin cermet layers and is not observed on thick anode used as the substrate in the ASC configuration. In this case, the cermet remains unconstrained and free to expand in such way that the porosity tends to increase upon re-oxidation.

(ii) Furthermore, the level of compressive stresses in the thin film of porous Ni/YSZ could be significantly overestimated con-

sidering the available data related to as-manufactured Ni/YSZ substrates. For instance, Pihlatie et al. [25] reported that 'redox' cycling involved a damaging of their anode that is correlated with a decrease in the Young's modulus.

On the other hand, interfacial toughness G_c has to be measured for the bi-material considered. Unfortunately, experimental data for the cermet/YSZ interface are not available. Sarantaridis et al. [18] have evaluated the interfacial energy to 10 J m^{-2} by considering the bulk toughness of 8YSZ reduced by the effect of cermet porosity. However, some results tend to indicate that the adhesion energy between porous electrode and electrolyte would be higher. Interfacial toughness of the electrolyte/cathode bi-material [26] (where the cathode is a porous composite of 8YSZ and LSM) has been estimated to around 20 J m^{-2}. Moreover, preliminary results obtained by micro-indentation on YSZ//Ni-YSZ system tend to confirm that the interfacial energy is even higher than this value. The analysis of these results is on-going and will be soon published.
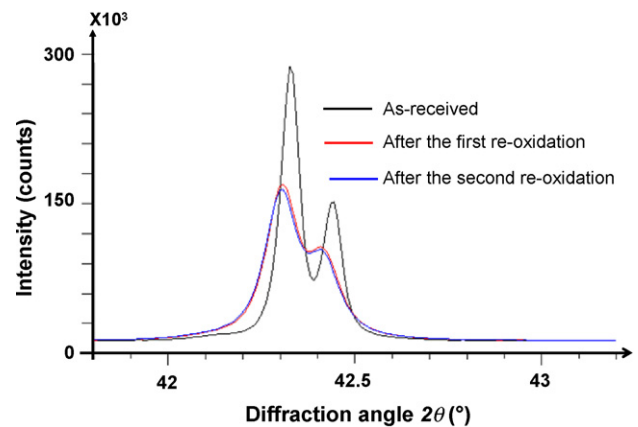

Fig. 9. X-ray diffractograms of anodic cermet (NiO (0 1 2) reflection): (i) black curve: as received (after manufacturing), (ii) red curve: after the first re-oxidation, and (iii) blue curve: after the second re-oxidation. (For interpretation of the references to color in this figure legend, the reader is referred to the web version of the article.)
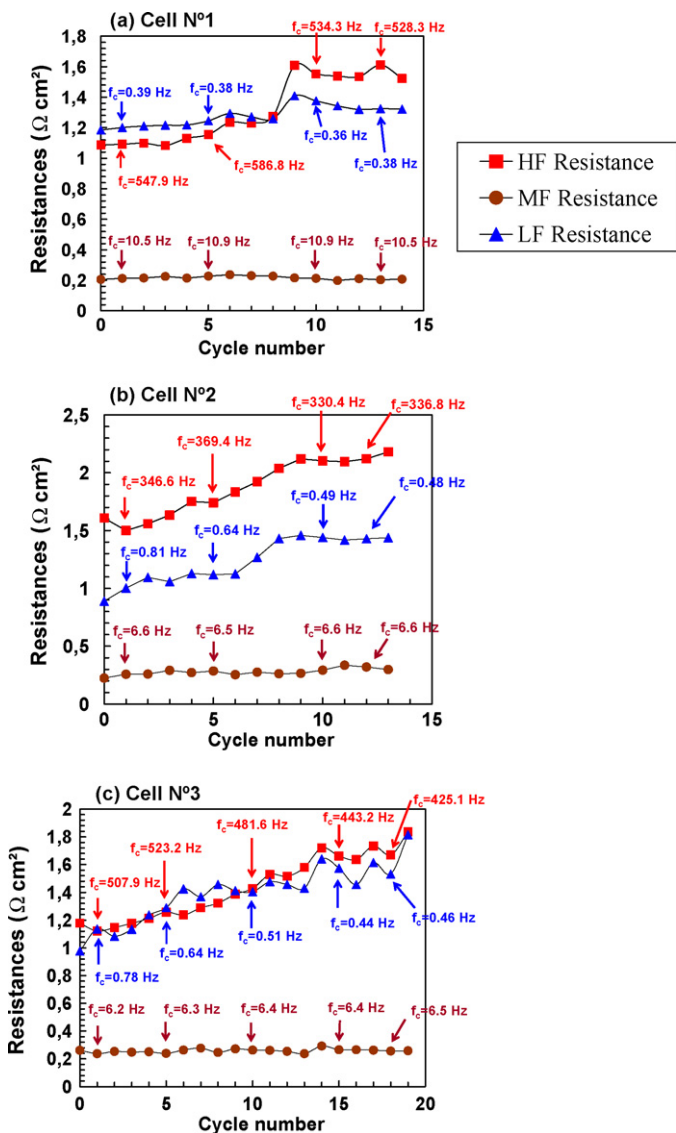
Fig. 10. High frequencies (HF), medium frequencies (MF) and low frequencies (LF) resistances plotted as a function of the cycle number for the three tested cells. The characteristic frequencies f_c of the HF, MF and LF semicircles have been added in the graphs.

As a consequence, it can be assumed at this step that the anode delamination may be hindered in the ESC configuration because of:

(i) an accommodation of compressive stress associated to a cermet microstructure re-arrangement (coarsening, micro-cracking), that would lower the amount of stored energy,
(ii) and a good adhesion between the materials, that would result in an high interfacial toughness.

Furthermore, as the anode is purely constituted by Ni and YSZ, no reactivity can occur with the electrolyte. Therefore, the interfacial toughness is not expected to be lowered after the cell ageing in operation. This remark means that the present analysis remains valid even after a long term operation.

4.2. Cermet bulk damage

Attempts to link the increase in the cell polarisation resistance with the cermet microstructure evolution during the 'redox' cycles is proposed hereafter. Fig. 10 shows separately the evolutions of

R_{HF}, R_{MF} and R_{LF} resistances plotted as a function of the cycle number. The characteristic frequencies f_c associated to each semicircle have also been added in the graphs. A good consistency is obtained between the results of the impedance diagrams fit. The same evolution is observed for the three tested cells, that tends to validate the approach.

As expected, only the first and the last semicircles ranging respectively at high and low frequencies have grown upon 'redox' cycles. The resistance and the characteristic frequency of the second semicircle, which was not sensitive to hydrogen partial pressure modification, remain nearly stable all over the test.

It can be noticed in Fig. 10 that the progressive increase in the HF and LF semicircles occurs without significant modification of their respective characteristic frequency. As the peak of frequency of both semicircles is remained roughly unchanged, it can be inferred that there has been no change in the basic electrochemical mechanisms during the tests. This remark involves that the impedance diagram evolutions are mainly caused by a modification of geometrical parameters that govern these mechanisms. These changes can be correlated with the cermet re-arrangement:

(i) The characteristic frequencies associated to the last semicircle are found to be equal to around 1/2 Hz for the three tested cells. This low value is usually attributed to a limitation by gas conversion and gas diffusion [27,28]. Therefore, the increase in size of the related semicircle seems to be consistent with the densification of the microstructure which must hinder the mass transport inside the electrode.
(ii) The average characteristic frequency associated with the first semicircle is equal to 460 Hz. According to previous studies [21,29–31], this anodic contribution involved in the HF semicircle can be attributed to the charge transfer reaction, namely the electrochemical oxidation of hydrogen. This reaction takes places at the triple phase boundaries (TPBs) defined by the line where the gas meets both electrolyte and nickel phase. Therefore, increase in the polarisation resistance associated to the HF semicircle could be ascribed with a reduction in the amount of TPBs length. This explanation is consistent with the observed cermet microstructure densification and Ni agglomeration which must lead to a decrease in active sites for the hydrogen oxidation.

In the present paper, it has been highlighted that the bulk anode degradation caused by the 'redox' cycles affects the semicircles constituting the impedance diagrams. In another study [17], it has been shown that the anode/electrolyte interface delamination has also a strong impact on the diagrams. Therefore, the impedance spectroscopy appears to be an efficient tool to separate the different mechanisms of cell degradation.

This technique could be applied to state on the reliability of some recommendations done to avoid the damage induced by the 'redox' cycles. For instance, it has been proposed to lower the amount of Ni content in such way that the cermet expansion is reduced: Busawon et al. [32] have investigated the Ni infiltration on porous YSZ structure, whereas Waldbillig et al. [33] have manufactured cells with functionally graded AFL presenting a lower amount of Ni near the electrolyte. According to the present result, it appears that the 'redox' tolerance could be enhanced by the stabilisation of the cermet microstructure. In this condition, cermets which have been optimised to prevent the Ni agglomeration could withstand a higher number of 'redox' cycles. It has been shown by Tietz and Nikolopoulos [34] that the stabilisation of the cermet regarding the Ni coarsening could be achieved by addition of Ti in the 8YSZ phase. This improvement has been attributed to a better adhesion between the Ni and the ceramic phase. Therefore, it will be relevant to check if such materials could hinder the cermet re-arrangement

induced by the 'redox' cycle. The polarisation resistance of such improved cermets should be more stable and this effect could be quantified by impedance spectroscopy.

5. Conclusion

The degradation of an electrolyte supported cell (ESC) upon redox cycling has been followed *in situ* by electrochemical impedance spectroscopy (EIS). It has been shown that the evolutions in impedance spectra, continuously recorded, are representative for a structural degradation spreading through the volume of the Ni/YSZ electrode. The interpretation of EIS results has been found to be well correlated with the microstructure change:

(i) Densification and coarsening of the cermet microstructure shown by SEM,
(ii) Widening of diffraction peak of the NiO phase observed by DRX after 'redox' cycling.

On the other hand, electrode delamination has not been observed between cermet and electrolyte in spite of the Ni particles swelling upon oxidation. It has been proposed that compressive stresses inside the cermet may be accommodated by the microstructure changes of the thin Ni-YSZ film.

It has been stated that the methodology constitutes an efficient tool to investigate the mechanisms and also to diagnostic the causes of cell degradation. Indeed, different modes of cell degradation: (i) carbon deposition [35], (ii) delamination [17] and (iii) now bulk cermet coarsening can be identified. This technique is also a promising approach to analyse the specific degradation of solid oxide electrolysis cells which constitutes an emerging application of this technology.

References

[1] S.C. Singhal, K. Kendall, in: S.C. Singhal, K. Kendall (Eds.), High Temperatures Solid Oxide Fuel Cells, Elsevier, Oxford, 2003, p. 17.
[2] M. Suzuki, T. Sogi, K. Higaki, T. Ono, N. Takahashi, K. Shimazu, T. Shigehisa, ECS Trans. 7 (1) (2007) 27.
[3] D. Fouquet, A.C. Müller, A. Weber, E. Ivers-Tieffée, Ionics 8 (2003) 103.
[4] D. Waldbillig, A. Wood, D.G. Ivey, Solids State Ionics 176 (2005) 847.
[5] T. Klemenso, C. Chung, P.H. Larsen, M. Mogensen, J. Electrochem. Soc. 152 (11) (2005) A2186.
[6] D. Sarantaridis, R.J. Chater, A. Atkinson, J. Electrochem. Soc. 155 (5) (2008) B467.
[7] M. Cassidy, G. Lindsay, K. Kendall, J. Power Sources 61 (1996) 189.
[8] M. Ettler, G. Blaß, N.H. Menzler, Fuel Cells 7 (5) (2007) 349.
[9] J. Malzbender, E. Wessel, R.W. Steinbrech, Solid State Ionics 176 (2005) 2201.
[10] T. Klemenso, C. Chung, P.H. Larsen, M. Mogensen, in: S.C. Singhal, J. Mizusaki (Eds.), In Solid Oxide Fuel Cells IX, ECS Proc., 2005, p. 1226.
[11] D. Waldbillig, A. Wood, D.G. Ivey, J. Power Sources 145 (2005) 206.
[12] J. Kong, K. Sun, D. Zhou, N. Zhang, J. Qiao, Rare Metals 25 (2006) 300.
[13] B. Liu, Y. Zhang, B. Tu, Y. Don, M. Cheng, J. Power Sources 165 (2007) 114.
[14] M.C Tucker, G.Y. Lau, C.P. Jacobson, L.C. De Jonghe, S.J. Visco, J. Power Sources 175 (2008) 447.
[15] J. Laurencin, G. Delette, F. Lefebvre-Joud, M. Dupeux, J. Eur. Ceram. Soc. 28 (2008) 1857.
[16] D. Sarantaridis, R.A. Rudkin, A. Atkinson, J. Power Sources 180 (2008) 704.
[17] J. Laurencin, G. Delette, F. Lefebvre-Joud, M. Dupeux, J. Power Sources 192 (2009) 344.
[18] D. Sarantaridis, A. Atkinson, 7th European Fuel Cell Forum (Switzerland) Paper P0728, 2006.
[19] D. Sarantaridis, A. Atkinson, Fuel Cells 3 (2007) 246.
[20] A.C. Müller, A. Krüger, E. Ivers-Tieffée, in: S.C. Singhal, M. Dokiya (Eds.), Solid Oxide Fuel Cells VIII, ECS Proc., 7, 2003, p. 680.
[21] T.L. Reitz, H. Xiao, J. Power Sources 161 (2006) 437.
[22] J.I. Gazzari, O. Kesler, J. Power Sources 167 (2007) 100.
[23] J.I. Gazzari, O. Kesler, J. Power Sources 167 (2007) 430.
[24] J.I. Gazzari, O. Kesler, J. Power Sources 176 (2008) 138.
[25] M. Pihlatie, A. Kaiser, M. Mogensen, J. Eur. Ceram. Soc. 29 (2009) 1657.
[26] G. Delette, J. Laurencin, M. Dupeux, J.B. Doyer, Scripta Mater. 59/1 (2008) 31.
[27] M. Mogensen, P. Vang Hendriksen, in: S.C. Singhal, K. Kendall (Eds.), High Temperatures Solid Oxide Fuel Cells, Elsevier, Oxford, 2003, p. 283.
[28] S. Primdhal, M. Mogensen, J. Electrochem. Soc. 145 (7) (1998) 2431.
[29] S. Primdhal, M. Mogensen, J. Electrochem. Soc. 144 (10) (1997) 3409.
[30] M. Guillodo, P. Vernoux, J. Fouletier, Solid State Ionics 127 (2000) 99.
[31] M. Lang, C. Auer, A. Eismann, P. Szabo, N. Wagner, Electrochim. Acta 53 (2008) 7509.
[32] A.N. Busawon, D. Sarantaridis, A. Atkinson, Electrochem. Solid-State Lett. 11 (10) (2008) B186.
[33] D. Waldbillig, A. Wood, D.G. Ivey, J. Electrochem. Soc. 154 (2) (2007) B133.
[34] F. Tietz, P. Nikolopoulos, Fuels Cells (in press) DOI:10.1002/fuce.200800125.
[35] J. Laurencin, K. Girona, G. Delette, F. Lefebvre-Joud, ECS Trans. 25 (2) (2009) 429.